Journal of Alloys and Compounds 505 (2010) 23–28

Contents lists available at ScienceDirect

Journal of Alloys and Compounds

journal homepage: www.elsevier.com/locate/jallcom

Electrical resistivity and magnetic properties of Nd–Fe–B alloys produced by melt-spinning technique

Tetsuji Saito

Department of Mechanical Science and Engineering, Chiba Institute of Technology, 2-17-1 Tsudanuma, Narashino, Chiba 275-0016, Japan

ARTICLE INFO

Article history:
Received 30 April 2010
Received in revised form 15 May 2010
Accepted 21 May 2010
Available online 19 June 2010

Keywords:
Nd–Fe–B magnets
Electrical resistivity
Magnetic properties
Melt-spinning

ABSTRACT

The electrical resistivity and magnetic properties of Nd–Fe–B alloys produced by the melt-spinning technique were examined. The wheel speed, which is closely associated with the cooling rate, was varied in the production of the melt-spun ribbons. The resultant melt-spun ribbons had various microstructures ranging from dendrite to equiaxed grains, and finally to an amorphous structure, depending on the wheel speed. It was found that both the resistivity and coercivity of the melt-spun ribbons were strongly dependent on the wheel speed. The maximum resistivity of 3.15 μΩ m was achieved in a melt-spun ribbon primarily consisting of the amorphous phase with a small amount of the $Nd_2Fe_{14}B$ phase, while the highest coercivity of 1.97 MA/m was achieved in a melt-spun ribbon primarily consisting of the $Nd_2Fe_{14}B$ phase with a small amount of the amorphous phase. The relationships among the cooling rate, microstructure, resistivity, and coercivity of the Nd–Fe–B alloys were determined.

1. Introduction

Neodymium–iron–boron (Nd–Fe–B) magnets with outstanding magnetic properties have been produced either from comminuted rapidly solidified melt-spun ribbons, as bonded or hot-formed magnets, or by sintering after prior green compaction in an applied magnetic field [1–3]. The superiority of these magnets arises from the $Nd_2Fe_{14}B$ intermetallic compound, which has a large saturation magnetization and a high anisotropy field [4,5]. The actual magnetic properties of Nd–Fe–B magnets are strongly dependent on their microstructures, particularly the grain size of the $Nd_2Fe_{14}B$ phase and the grain boundary phases. As a consequence of intensive studies, the maximum energy product of Nd–Fe–B magnets has been improved to the point where it has reached the practical limitations of these magnets [6–8]. Nd–Fe–B magnets are now widely used in various applications such as voice coil motors (VCMs) in hard disk drives and driving motors for hybrid and electrical vehicles due to their high energy product and relatively low cost.

In permanent magnets used for driving motors in hybrid and electrical vehicles, eddy-current loss has become a major problem [9–11]. Since the electrical resistivity of Nd–Fe–B magnets is relatively low, considerable eddy-current loss is generated by the magnetic fields in the motor. This may cause a substantial temperature rise and result in partial irreversible demagnetization of the magnets, especially in motors with high electrical loading, a high rotational speed, or a high pole number. It has been reported that the oxidation resistance of Nd–Fe–B magnets is dependent on the microstructure [12]. The electrical resistivity of these magnets is also believed to be dependent on the microstructure, especially the grain size of the $Nd_2Fe_{14}B$ phase. Therefore, it is important to evaluate the electrical resistivity of Nd–Fe–B magnets.

In this study, Nd–Fe–B alloys with various grain sizes of the $Nd_2Fe_{14}B$ phase were produced by the melt-spinning technique, and their electrical resistivity and magnetic properties were examined. The relationships among the structures, electrical resistivity, and magnetic properties of these Nd–Fe–B alloys are discussed.

2. Experiment

$Nd_{15}Fe_{77}B_8$ alloy ingots were produced by induction melting in an argon atmosphere. Small amounts of the ingots were placed in a quartz crucible with an orifice of 0.6 mm at the bottom. The alloy ingots were induction melted in an argon atmosphere and then ejected through the orifice with argon onto a chromium-plated copper wheel rotating at a surface velocity of 5–25 ms^{-1}. The phases of the specimens were examined by X-ray diffraction (XRD) using Cu Kα radiation. The thermal properties of the specimens were measured in an argon atmosphere using a differential scanning calorimeter (DSC). The microstructures of the specimens were examined using a scanning electron microscope (SEM) after polishing and etching with 1% Nital. The magnetic properties of the specimens were measured by a vibrating sample magnetometer (VSM) with a maximum applied field of 2.0 MA/m after the specimens had been magnetized at a pulsed field of 4.0 MA/m. The VSM was calibrated with a pure nickel sphere. The electrical resistivity of the specimens was measured at room temperature using the four-probe method. The temperature dependence of the electrical resistivity of the specimens was then measured at temperatures from 20 K to 300 K in a helium atmosphere.

E-mail address: tetsuji.saito@it-chiba.ac.jp.

0925-8388/$ – see front matter © 2010 Elsevier B.V. All rights reserved.
doi:10.1016/j.jallcom.2010.05.175

3. Results and discussion

Fig. 1 shows the XRD patterns of the Nd–Fe–B melt-spun ribbons produced at various wheel speeds. The XRD pattern of the melt-spun ribbon produced at a wheel speed of 5 m/s is well indexed to the tetragonal $Nd_2Fe_{14}B$ phase. This indicates that the specimen contains the $Nd_2Fe_{14}B$ phase. According to the phase diagram, the $Nd_2Fe_{14}B$ phase should coexist with other phases such as the Nd and $Nd_{1.1}Fe_4B_4$ phases in $Nd_{15}Fe_{77}B_8$ alloy [13]. However, no clear diffraction peaks of other phases are found in the XRD pattern. This is due to the relatively small fractions of the other phases in the $Nd_{15}Fe_{77}B_8$ alloy. The diffraction peaks of the $Nd_2Fe_{14}B$ phase become smaller and broader as the wheel speed increases. The XRD pattern of the melt-spun ribbon produced at a wheel speed of 20 m/s shows no evidence of these peaks, but instead exhibits a fairly broad halo-like peak at $2\theta = 30$–50°. This broad halo is characteristic of an amorphous structure, indicating that the melt-spun ribbon is essentially in the amorphous state. Virtually the same XRD pattern is obtained from the melt-spun ribbon produced at a wheel speed of 25 m/s. It is known that the wheel speed is closely related to a cooling rate in the melt-spinning technique. However, direct measurement of the cooling rate is extremely difficult because of the high cooling rate attained with this technique. The wheel speed is therefore used as the measure of the cooling rate in most melt-spinning experiments. The estimated cooling rates of the melt-spun ribbons produced at wheel speeds of 5 m/s and 25 m/s are around 1×10^{-5} K/s and around 1×10^{-6} K/s, respectively [14]. A higher wheel speed—that is to say, a higher cooling rate attained by the melt-spinning technique—could promote formation of the amorphous phase in preference to the $Nd_2Fe_{14}B$ phase.

Fig. 2 shows the DSC curves of the Nd–Fe–B melt-spun ribbons. The curve of the melt-spun ribbon produced at a wheel speed of 5 m/s shows a small endothermic peak at about 590 K, corresponding to the Curie temperature of the ferromagnetic $Nd_2Fe_{14}B$ phase [5]. This confirms that the melt-spun ribbon consists of the $Nd_2Fe_{14}B$ phase. In the DSC curve of the ribbon produced at a wheel speed of 10 m/s, a small exothermic peak is exhibited at around 850 K together with the endothermic peak corresponding to the Curie temperature of the $Nd_2Fe_{14}B$ phase. The exothermic peak is considered to be the crystallization of the $Nd_2Fe_{14}B$ phase from the amorphous Nd–Fe–B materials. After DSC measurement, the XRD patterns of the melt-spun ribbons were well indexed to the $Nd_2Fe_{14}B$ phase. Therefore, the exothermic peak in the DSC curves corresponds to the crystallization temperature of the $Nd_2Fe_{14}B$ phase from the amorphous phase. The DSC studies thus revealed the existence of the amorphous phase in the melt-spun ribbon produced at a wheel speed of 10 m/s. Virtually the same DSC curve was obtained from the melt-spun ribbon produced at a wheel speed of 15 m/s, suggesting that the ribbon consisted of the $Nd_2Fe_{14}B$ phase together with a small amount of the amorphous phase. According to the XRD studies, the melt-spun ribbon produced at a wheel speed of 20 m/s was essentially in the amorphous state. However, the corresponding DSC curve still shows the endothermic peak of the $Nd_2Fe_{14}B$ phase together with the exothermic peak, which is larger than that of the melt-spun ribbon produced at a wheel speed of 15 m/s. This suggests that the melt-spun ribbon produced at a wheel speed of 20 m/s still contains a small amount of the $Nd_2Fe_{14}B$ phase together with the amorphous phase. During melt-spinning, first the $Nd_2Fe_{14}B$ phase precipitates from the melt, which becomes enriched in Nd, and then the remaining Nd-rich liquid may solidify into an amorphous phase [15]. Thus, the amount of the amorphous phase increases as the cooling rate, in this case the wheel speed, increases. A fully amorphous material was obtained in the melt-spun ribbon produced at a wheel speed of 25 m/s.

Fig. 3 shows scanning electron micrographs of the Nd–Fe–B melt-spun ribbons. The melt-spun ribbon produced at a wheel speed of 5 m/s consists of dendritic grains with an average grain size of 1 μm. Such a dendritic structure is often found in the Nd–Fe–B melt-spun ribbon produced at low wheel speeds [16–18]. Analysis by electron probe microanalyzer (EPMA) revealed that the grains were the $Nd_2Fe_{14}B$ phase. On the other hand, the melt-spun rib-

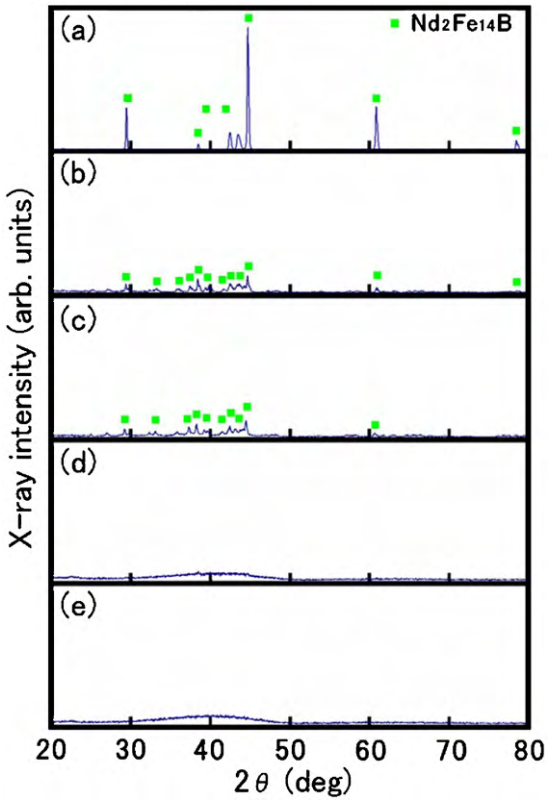

Fig. 1. XRD patterns of the Nd–Fe–B melt-spun ribbons produced at wheel speeds of (a) 5 m/s, (b) 10 m/s, (c) 15 m/s, (d) 20 m/s, and (e) 25 m/s.

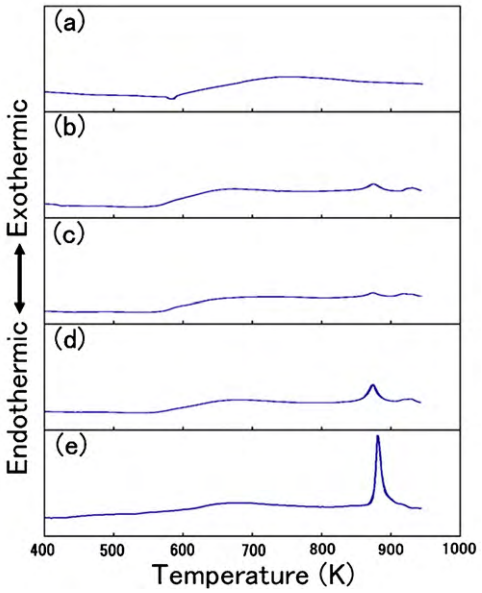

Fig. 2. DSC curves of the Nd–Fe–B melt-spun ribbons produced at wheel speeds of (a) 5 m/s, (b) 10 m/s, (c) 15 m/s, (d) 20 m/s, and (e) 25 m/s.

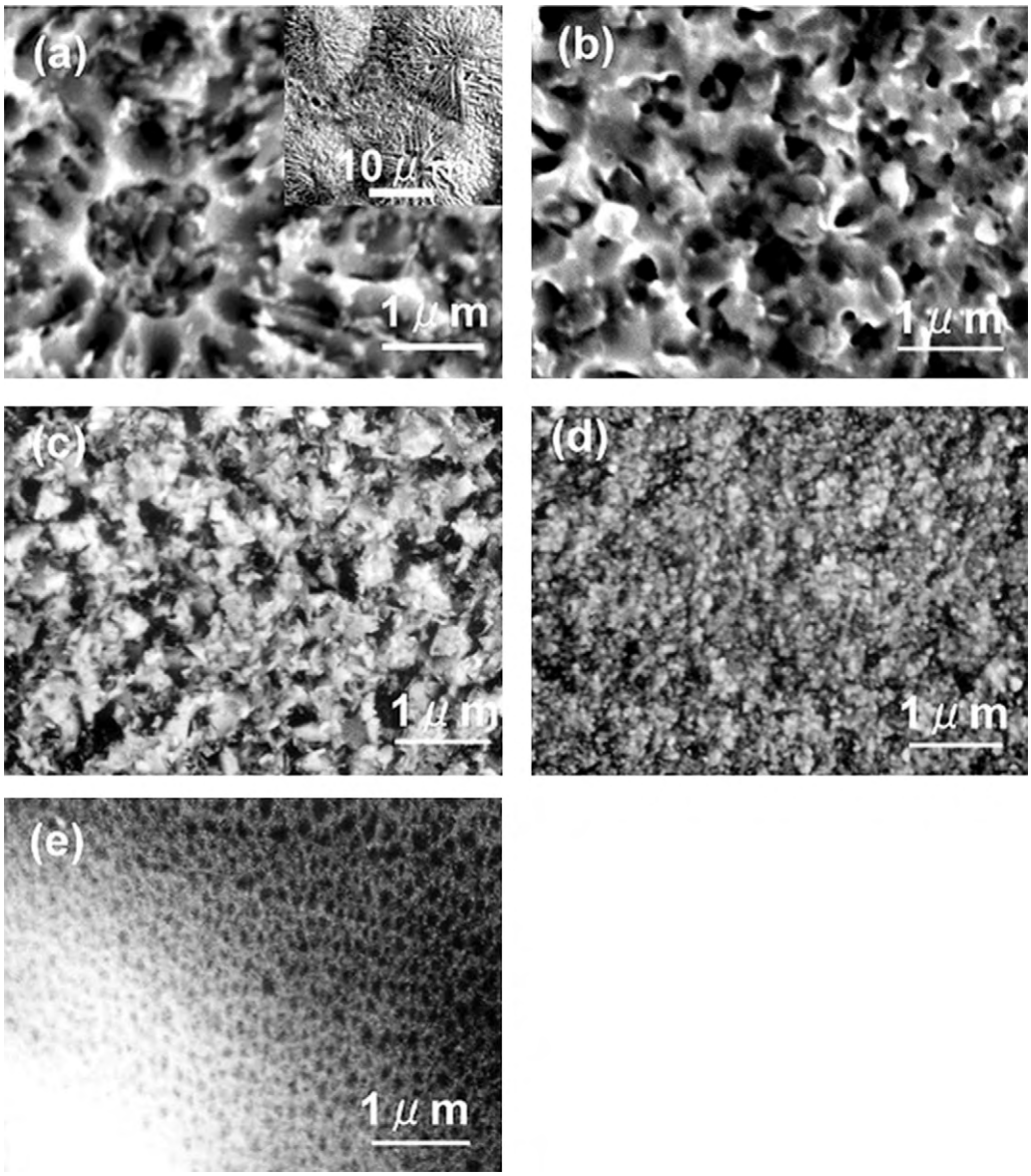

Fig. 3. Scanning electron micrographs of the Nd–Fe–B melt-spun ribbons produced at wheel speeds of (a) 5 m/s, (b) 10 m/s, (c) 15 m/s, (d) 20 m/s, and (e) 25 m/s. The insect in micrograph (a) shows a low-magnification image of the melt-spun ribbon produced at a wheel speed of 5 m/s.

bon produced at a wheel speed of 10 m/s consists of equiaxed grains with an average grain size of about 0.3 μm. The transition of the microstructure from dendrites to equiaxed grains results from the increased cooling rate associated with higher wheel speed. This type of microstructural transition has been noted by several researchers working with various ferrous and nonferrous alloys [19–21]. In all alloys studied, dendritic morphologies, which formed at low undercoolings, were replaced with randomly oriented "spherical elements" or fine grains at large undercoolings [21]. Thus, the fine-grain structures obtained in the specimens produced at high wheel speeds are considered to have resulted from a high degree of undercooling in the melt prior to nucleation. As the wheel speed increases, the grain size of the $Nd_2Fe_{14}B$ phase in the melt-spun ribbon becomes smaller and smaller. The melt-spun ribbon produced at a wheel speed of 20 m/s consists of fine equiaxed grains with an average grain size of less than 0.1 μm. In order to clarify the grain size of the melt-spun ribbon produced at a wheel speed of 20 m/s, further microstructural studies were performed by transmission electron microscope (TEM). The results are shown in Fig. 4. It was found that the actual grain size of the $Nd_2Fe_{14}B$ phase, which was embedded in the amorphous matrix, was around 20 nm. This is consistent with the results of the DSC studies. The microstructure of the melt-spun ribbon produced at a wheel speed of 25 m/s is somewhat featureless and no clear grains are seen in the micrograph. This indicates that the ribbon consists of amorphous materials. No crystallites were found in the TEM micrograph of the melt-spun ribbon, and the featureless region was identified to be the amorphous by electron diffraction. This indicates that a further increase in the wheel speed resulted in the transition of the microstructure from fine equiaxed grains to the amorphous phase.

Fig. 5 shows the hysteresis curves of the Nd–Fe–B melt-spun ribbons. Since the applied field of 2.0 MA/m is far below the filed required to fully saturate the specimen, the hysteresis curve is not closed (i.e., it is a minor loop), and it is not symmetrical with respect to either coordinate. The hysteresis curves consequently show an almost linear slope in the second quadrant with a relatively low remanence. Thus, the magnetic property of particular

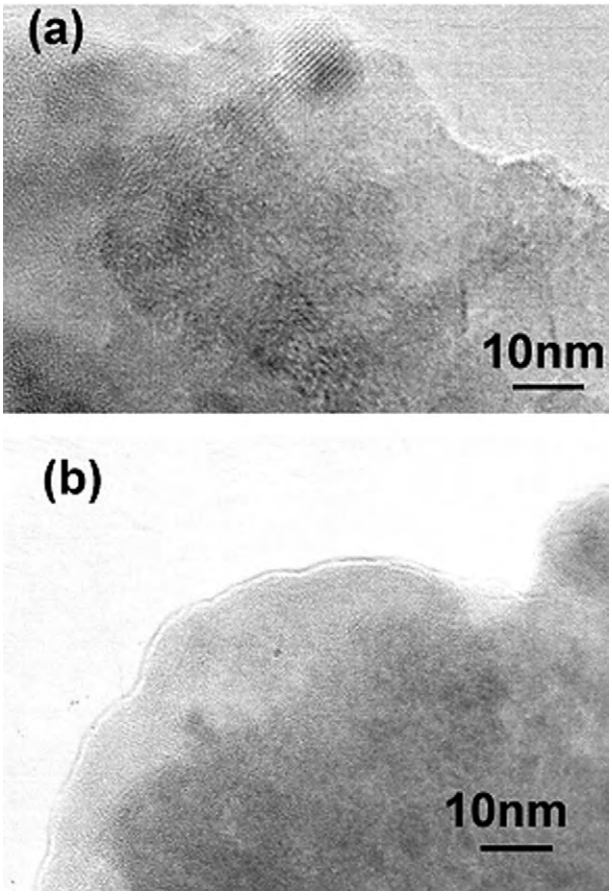

Fig. 4. Transmission electron micrographs of the Nd–Fe–B melt-spun ribbons produced at wheel speeds of (a) 20 m/s and (b) 25 m/s.

interest in this study was the coercivity, which is strongly related to the cooling rate. The coercivity of the melt-spun ribbon produced at a wheel speed of 5 m/s is 1.25 MA/m, much higher than that of the Nd–Fe–B alloy ingot, which is typically less than 0.1 MA/m. The observed high coercivity is due to the fine equiaxed $Nd_2Fe_{14}B$ grains in the melt-spun ribbon. The ribbons produced at a wheel speed of 10 m/s shows a high coercivity of 1.97 MA/m, while that produced at a wheel speed of 15 m/s also shows a high coercivity of 1.82 MA/m. Due to their fine equiaxed $Nd_2Fe_{14}B$ grain, these melt-spun ribbons exhibit an attractively high coercivity value [22]. A small kink is noted in the hysteresis curve of the specimen produced at a wheel speed of 15 m/s, suggesting that the melt-spun ribbon consists of two magnetic phases with different coercivity. According to the XRD and DSC studies, the melt-spun ribbon consisted mostly of the $Nd_2Fe_{14}B$ phase and a small amount of the amorphous phase. The presence of a small amount of the amorphous phase gives rise to the observed kink, which is not desirable in the hysteresis curve. On the other hand, the hysteresis curve of the melt-spun ribbon produced at a wheel speed of 20 m/s shows a "constricted" shape. Such a shape is characteristic of the coexistence of soft and hard magnetic phases in an alloy [22]. In this case, the soft and hard magnetic phases are the amorphous Nd–Fe–B and $Nd_2Fe_{14}B$ phases, respectively. Thus, the increase of amorphous Nd–Fe–B materials gives rise to the observed drastic changes in the hysteresis curve. The hysteresis curve of the melt-spun ribbon produced at a wheel speed of 25 m/s shows a typical hysteresis curve with a low coercivity value for soft magnetic materials. This confirms that the melt-spun ribbon consists of amorphous Nd–Fe–B materials.

Fig. 6 shows the dependence of the electrical resistivity of the Nd–Fe–B melt-spun ribbons on the wheel speed. The electrical resistivity was measured at room temperature. The melt-spun ribbon produced at a wheel speed of 5 m/s shows a resistivity of 1.43 μΩ m. This value is almost comparable to that of the Nd–Fe–B sintered magnets [23], but it is slightly larger than that of the Nd–Fe–B alloy ingot of 1.16 μΩ m. The reason for this is the finer grain size of the melt-spun ribbon compared with that of the Nd–Fe–B alloy ingot, which is typically around 20-50 μm. This confirms that the resistivity is dependent on the grain size of the $Nd_2Fe_{14}B$ phase. The resistivity of the melt-spun ribbon first increases and then decreases as the wheel speed increases. In the case of coercivity, the maximum value was obtained in the melt-spun ribbon consisting of fine $Nd_2Fe_{14}B$ grains with a small amount of the amorphous phase. In contrast, the maximum electrical resistivity value of 3.15 μΩ m was obtained in the melt-spun ribbon produced at a wheel speed of 20 m/s, which consisted of a mixture of the fine $Nd_2Fe_{14}B$ and amorphous phases. This implies that the resistivity of the melt-spun ribbon is dependent on the amount of the amorphous phase. The resistivity of amorphous materials is generally considered to be quite large because the mean free path of the electrons is short [24]. However, the amorphous melt-spun ribbon produced at a wheel speed of 25 m/s shows a slightly lower resistivity than that produced at a wheel speed of 20 m/s consisting of a mixture of the fine $Nd_2Fe_{14}B$ and amorphous phases. Thus, the resistivity of the melt-spun ribbon is considered to be dependent on the grain size of the $Nd_2Fe_{14}B$ phase in the ribbon.

Detailed electrical resistivity studies of the Nd–Fe–B melt-spun ribbons were carried out at temperatures from 20 K to 300 K. The results are shown in Fig. 7. In the melt-spun ribbon produced at a wheel speed of 5 m/s, the resistivity decreases as the temperature decreases. This is the typical temperature dependence of resistivity, as seen in ordinal metals such as Fe and Cu [25,26]. The temperature coefficient of the resistivity of the melt-spun ribbon becomes smaller as the wheel speed increases. The absolute resistivities of the melt-spun ribbons produced at wheel speeds of 10 m/s and 15 m/s are higher than that of the ribbon produced at a wheel speed of 5 m/s. Since these melt-spun ribbons consisted of the fine $Nd_2Fe_{14}B$ phase together with a small amount of the amorphous phase, the increased resistivity of these melt-spun ribbons is partly due to the additional electron scattering on the grain boundaries of the fine grains and partly due to the existence of a small amount of the amorphous phase. On the other hand, the resistivity of the melt-spun ribbon produced at a wheel speed of 20 m/s, which consisted of a mixture of the fine $Nd_2Fe_{14}B$ and amorphous phases, increases as the temperature decreases. This implies that the amorphous phase possesses a negative temperature coefficient of resistivity and consequently exhibits a negative temperature dependence due to the large amount of the amorphous phase in the melt-spun ribbon. However, the resistivity of the melt-spun ribbon produced at a wheel speed of 25 m/s, which consisted of the amorphous phase, shows virtually no temperature dependence. Thus, the observed negative temperature coefficient of the resistivity of the ribbon consisting of a mixture of the fine $Nd_2Fe_{14}B$ and amorphous phases is not due to the amorphous phase but to the fine $Nd_2Fe_{14}B$ phase. It has been reported that nanocrystalline materials exhibit higher resistivity than polycrystalline metals [27]. The above results suggest that Nd–Fe–B ribbon having a high coercivity over 1.8 MA/m with electrical resistivity comparable to the amorphous Nd–Fe–B phase can be produced by the melt-spinning technique. A further increase in the electrical resistivity of Nd–Fe–B melt-spun ribbon may be attained by decreasing the grain size of the $Nd_2Fe_{14}B$ phase without increasing the amount of the amorphous phase.

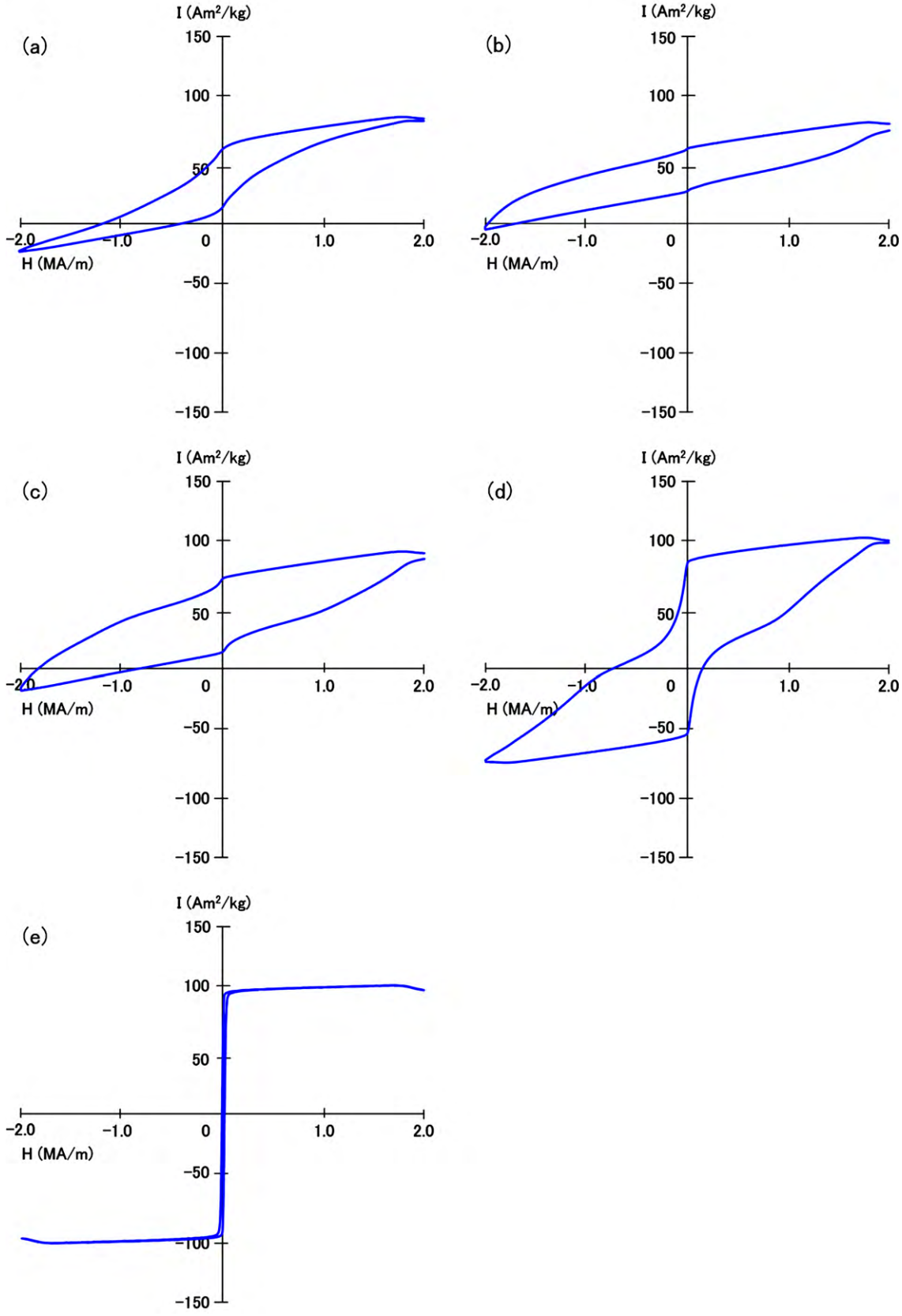

Fig. 5. Hysteresis curves of the Nd–Fe–B melt-spun ribbons produced at wheel speeds of (a) 5 m/s, (b) 10 m/s, (c) 15 m/s, (d) 20 m/s, and (e) 25 m/s. Since the applied field of 2.0 MA/m is far below the filed required to fully saturate the specimen, the hysteresis curve is not closed (i.e., it is a minor loop), and it is not symmetrical with respect to either coordinate.

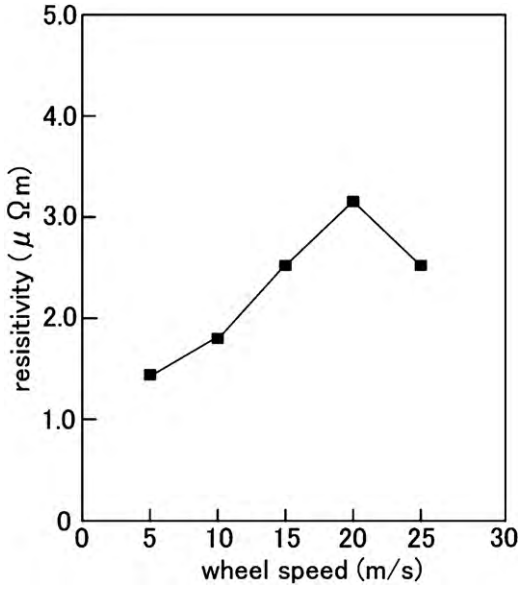

Fig. 6. Dependence of the electrical resistivity of the Nd–Fe–B melt-spun ribbons on the wheel speed. The electrical resistivity was measured at room temperature.

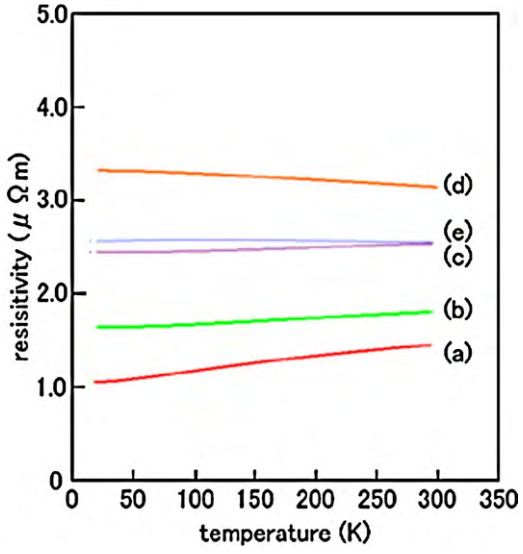

Fig. 7. Temperature dependence of the electrical resistivity of the Nd–Fe–B melt-spun ribbons produced at wheel speeds of (a) 5 m/s, (b) 10 m/s, (c) 15 m/s, (d) 20 m/s, and (e) 25 m/s.

4. Conclusion

Nd–Fe–B alloy ribbons were produced by the melt-spinning technique at various wheel speeds. The microstructures, electrical resistivity, and magnetic properties were examined in terms of the wheel speed, which is closely associated with the cooling rate. The melt-spun ribbon produced at a wheel speed of 5 m/s had a dendritic structure and showed a resistivity of 1.43 μΩ m and a coercivity of 1.25 MA/m. The ribbon produced at a wheel speed of 10 m/s had equiaxed $Nd_2Fe_{14}B$ phases with a small amount of the amorphous phase and showed a resistivity of 1.81 μΩ m with the highest coercivity of 1.97 MA/m. On the other hand, the ribbon produced at a wheel speed of 20 m/s consisted of the amorphous phase together with the $Nd_2Fe_{14}B$ phase and showed the highest resistivity of 3.15 μΩ m with a coercivity of 0.73 MA/m. The ribbon produced at a wheel speed of 25 m/s consisted of the amorphous phase and showed a low coercivity of 0.08 MA/m with a relatively high resistivity of 2.53 μΩ m. It was found that the optimally high coercivity and resistance were achieved in the melt-spun ribbon produced at a wheel speed of 15 m/s, which consisted of fine equiaxed $Nd_2Fe_{14}B$ phases with a small amount of the amorphous phase.

References

[1] J.J. Croat, J.F. Herbst, R.W. Lee, F.E. Pinkerton, J. Appl. Phys. 55 (1984) 2078.
[2] M. Sagawa, S. Fujimura, N. Togawa, H. Yamamoto, Y. Matsuura, J. Appl. Phys. 55 (1984) 2083.
[3] R.W. Lee, E.G. Brewer, N.A. Schaffel, IEEE Trans. Mag. MAG-21, 1958 (1985).
[4] N.C. Koon, B.N. Das, M. Rubinstein, J. Tyson, J. Appl. Phys. 57 (1985) 4091.
[5] C. Abache, H. Oesterreicher, J. Appl. Phys. 57 (1985) 4112.
[6] K. de Kort, in: F.P. Missell, V. Villas-Boas, H.R. Rechenberg, F.J.G. Landgraf (Eds.), Proc. 14th Intl. Workshop on Rare Earth Magnets and Applications, World Scientific Pub. Co., 1996, p. 47.
[7] W. Rodewald, B. Wall, M. Katter, K. Üstüner, S. Steinmetz, in: G.C. Hadjipanayis, M.J. Bonder (Eds.), Proc. 17th Intl. Workshop on Rare Earth Magnets and Applications, Rinton Press, 2002, p. 25.
[8] T. Saito, M. Fujita, T. Kuji, K. Fukuoka, Y. Syono, J. Appl. Phys. 83 (1998) 6390.
[9] H. Toda, Z. Xia, J. Wang, K. Atallah, D. Howe, IEEE Trans. Mag. 40 (2004) 2104.
[10] K. Yamazaki, M. Shina, M. Miwa, J. Hagiwara, IEEE Trans. Mag. 44 (2008) 4269.
[11] N. Takahashi, H. Shinagawa, D. Miyagi, Y. Doi, K. Miyata, IEEE Trans. Mag. 45 (2009) 1234.
[12] T. Saito, J. Mater. Lett. 20 (2001) 209.
[13] G. Schneider, E.-T. Hening, G. Petzow, H.H. Stadelmaier, Z. Metallkd. 78 (1987) 694.
[14] S. Ozawa, T. Saito, T. Motegi, J. Alloys Compd. 363 (2004) 263.
[15] J. Wecker, L. Schultz, J. Appl. Phys. 62 (1987) 990.
[16] J.J. Becker, R.A. Overfelt, IEEE Trans. Mag. MAG-20, 1596 (1984).
[17] D. Dadon, Y. Grefen, M.P. Dariel, IEEE Trans. Mag. 23 (1987) 3605.
[18] A. Zaluska, Y. Xu, Z. Altounian, J.O. Strom-Olsen, Mater. Sci. Eng. A133 (1991) 819.
[19] J. Fehling, E. Scheil, Z. Metallkd. 53 (1962) 563.
[20] J.L. Walker, Physical Chemistry of Metallurgy, Interscience, New York, 1961, Pt.II, p. 845.
[21] T.Z. Kattamis, M.C. Fleminigs, Trans. AIME 236 1523 (1966).
[22] C.J. Yang, R. Ray, R.C. O'Handley, Mater. Sci. Eng. 99 (1988) 137.
[23] http://www.hitachi-metals.co.jp/prod/prod03/p03_01.html.
[24] S.R. Elliot, Physics of Amorphous Material, 2nd ed., Longman Scientific & Technical, U.K., 1990, p. 302.
[25] M.J. Laubitz, T. Matsumura, P.J. Kelly, Can. J. Phys. 54 (1976) 92.
[26] G.K. White, S.B. Woods, Phil. Trans. Roy. Soc. A 251 (1959) 281.
[27] K. Pękała, M. Pękała, Nanostruct. Mater. 6 (1995) 819.